

Reaction Mechanism of Low-Grade Phosphate Ore During Vacuum Carbothermal Reduction



QINGHUI WU, JUNQI LI, XIAODONG LV, BENJUN XV, CHAOYI CHEN,
and RUN HUANG

The non-isothermal kinetic method was used in this manuscript to obtain the reaction models by fitting the reduction ratio of low-grade phosphate ore and the volatilization ratio of phosphorus. And the reaction mechanism of vacuum carbothermal reduction of low-grade phosphate was investigated by combining XRD, SEM, EDS, chemical analysis, and FactSage7.2. $\text{Ca}_5(\text{PO}_4)_3\text{F}$ first reacted with a small amount of SiO_2 in the ore sample at 1080 °C to form $\text{Ca}_3(\text{PO}_4)_2$, CaSiO_3 , and SiF_4 (escaped in the form of gas). Then, $\text{Ca}_3(\text{PO}_4)_2$ was reduced by C. When the temperature reached approximately 1300 °C, a large number of $\text{Ca}_5(\text{PO}_4)_3\text{F}$ in ore sample began to react with C to form CaO , $\text{P}_2(\text{g})$, $\text{CO}(\text{g})$, and CaF_2 . Through the mutual verification of Coats-Redfern and Šatava-Šesták methods, it is concluded that the unitary reduction process was under the control of the shrinking core model, and the activation energy of unitary reduction was 74.54 ± 10.39 kJ/mol. The volatilization of P was under the control of the 3-D diffusion (anti-Jander), and the activation energy was 416.43 ± 1.81 kJ/mol.

<https://doi.org/10.1007/s11663-021-02117-6>

© The Minerals, Metals & Materials Society and ASM International 2021

I. INTRODUCTION

PHOSPHATE ore is a non-metallic mineral resource that cannot be regenerated, cannot be replaced, and has strategic significance. It is an important chemical raw material widely used in the phosphate industry, metallurgy, and agriculture.^[1] The phosphate ore resource of China was low, *i.e.*, the average grade is only 17 pct, which is one of the countries with the lowest average grade of phosphate ore.^[2] At present, low-grade phosphate ore is often enriched by mineral processing, and then subsequent production was carried out, though. But mineral processing will reduce the availability of phosphorus and produce a large number of tailings. Currently, 8 to 9.5 million tons of phosphate tailings will be produced in China every year. Because phosphate tailings mainly contain MgO , P_2O_5 , CaO , SiO_2 , Al_2O_3 , and Fe_2O_3 oxides, in addition, it also includes a trace of heavy metals (Cd, Cr, Pd, Hg, As, *etc.*), resulting in a great waste of resources and heavy metal pollution.^[3] Therefore, the comprehensive utilization of low-grade phosphate ore has become a hot spot in present studies.

Currently, there are three mature manufacturing technologies of phosphate, namely, wet phosphoric acid, thermal phosphoric acid, and kiln phosphoric acid.^[4,5] Wet phosphoric acid requires phosphorus concentrate, and its byproduct-phosphogypsum pollutes the environment greatly. Moreover, the thermal energy consumption and cost of thermal phosphoric acid with a long process (including crushing, electric furnace reduction, cooling tower, refining pot, and hydration process) are much higher.^[6,7] The issue was solved by kiln phosphoric acid, but there are also some problems in the process of kiln phosphoric acid, such as the kiln-ringing, burning loss of carbon, P_2O_5 desorption, and kiln body design. On this basis, some scholars^[8,9] have advanced a new process of melting phosphorus refining by reference to the process of smelting iron. The melting condition was favorable to heat and mass transfer and reduced energy consumption. Li *et al.* and Ma *et al.*^[10–14] have studied the process of melting reduction of phosphate ore and its kinetics and determined that the optimum process parameters of molten reduction phosphate ore were as follows: 1450 °C for 60 minutes, C excess coefficient was 1.5, and SiO_2/CaO ratio was 2.4. According to the kinetic fitting results, the melt reduction process was a first-order reaction with an apparent activation energy of 225.106 $\text{KJ}\cdot\text{mol}^{-1}$. Tang *et al.*^[15] studied the effect of oxide flux such as aluminum-silicon-magnesium on the melting reduction of phosphate ore and obtained the strengthening effect of three fluxes: silica > alumina > magnesium oxide. In addition, in view of applications of vacuum reduction in ilmenite

QINGHUI WU, JUNQI LI, XIAODONG LV, BENJUN XV, CHAOYI CHEN, and RUN HUANG are with the School of Materials and Metallurgy Guizhou University, Guiyang City, China, 550000. Contact e-mail: rhuang@gzu.edu.cn

Manuscript submitted July 17, 2020; accepted February 8, 2021.

Article published online March 11, 2021.

concentrate, MgO, SiO₂, Al₂O₃, ZnO, *etc.*, and non-vacuum carbothermal reduction in ZnO, Al₂O₃.^[16–19] Other scholars have put forward the treatment of vacuum carbothermal reduction method, which has proved that the method can effectively recover phosphorus from low-grade phosphate ore at lower temperature without pollution (the reduced yellow phosphorus was collected directly by the collector through the condensing tube under the action of the vacuum pump). Figure 1 shows variations in Gibbs free energy which may occur in the electric furnace process at different pressure. It can be seen that the initial temperature of each reaction decreased significantly with reduced pressure. Moreover, the vacuum method avoids the steps of gas washing tower and refined pot greatly shortens the technological process and reduced the energy consumption of reaction based on direct utilization of low-grade phosphate ore. Huang *et al.*^[20–22] studied the effects of temperature, pressure, and carbon dosage on low-grade phosphate ore during vacuum carbothermal reduction. It's concluded that compared to the reaction temperature of 1500 °C in the traditional thermal process, carbothermal reduction temperature can be reduced to 1250 °C from 1300 °C with an additional vacuum system. Furthermore, the thermodynamic behavior and reduction kinetics of Ca₅(PO₄)₃F were studied by Cao *et al.* and Li *et al.*^[23–27] The study's conclusion was Ca₅(PO₄)₃F gave priority to defluorination reaction with SiO₂ to form Ca₃(PO₄)₂. Then, Ca₃(PO₄)₂ was reduced by C to produce CaO, which bound SiO₂ to form silicate. Finally, F was discharged in the form of SiF₄ (g). But the reduction mechanism and kinetics of carbothermal reduction of low-grade phosphate ore in vacuum remain unclear. Consequently, this manuscript studied the non-isothermal kinetics and reduction process. This study is expected to lay a theoretical and experimental foundation for the comprehensive utilization of phosphate ore.

II. EXPERIMENT

A. Materials

The chemical compositions of the materials employed in this research are shown in Table I (The relative standard deviation of each component was not more than 3.6 pct). The main elements in phosphate ore are Ca, P, O, and Si, which are mainly in the form of Ca₅(PO₄)₃F and SiO₂ as the XRD diagram of raw ore shown in Figure 2. And the particle sizes of all materials used in this experiment are less than 74 μm.

B. Experimental Procedure

The vacuum carbon shirt-circuiting furnace used in this study is shown in Figure 3, which consists of vacuum system, furnace stack, control cubicle, electric power system, and water cooling system. The vacuum system includes a mechanical pump, a diffusion pump, and valves. Mechanical pump is used for pre-pumping vacuum of equipment. The mechanical pump and the

diffusion pump work together to maintain high vacuum during reduction. The furnace stack includes base, furnace lid, furnace wall (connects with the cooling water system), insulation layer, graphite heating element, graphite cushion, reduction device (graphite crucible), and condensing collection device (graphite condensing tube and sheet glass). The reduced yellow phosphorus was collected directly by the collector through the condensing tube under the action of the vacuum pump.

A previous study^[21] showed that in the process of carbothermal reduction of low-grade phosphate ore in vacuum, with constant temperature and pressure, the reduction efficiency became best at 14 pct carbon dosage. Therefore, firstly, weigh 20g of phosphate ore powder, 14 wt pct coke (2.8g), 4 wt pct binders (methyl-cellulose) (0.8g), and 3 wt pct distilled water (0.6g), respectively, which were mixed and stirred evenly. The mixed powder was pressed to form a block (the mass of a single sample was approximately 24.14g) under a pressure of 15 MPa, and then the block was put into a loft drier to be dried for 8 hours at 105 °C. The dried samples were weighed and then heated to 1100 °C, 1150 °C, 1200 °C, 1250 °C, 1300 °C, 1350 °C, and 1400 °C, respectively, in the vacuum carbon shirt-circuiting furnace. The heating rate was set to 6 °C/min. When the temperature reached the set value, heating was stopped immediately and the samples were cooled in furnace (as shown in Figure 4, the cooling rate was 13.3 °C /min at 1000 °C to 1500 °C, 6.15 °C /min at 500 °C to 1000 °C, and 3°C /min below 500 °C). The accuracy of tungsten-rhenium thermocouples (WER-526) and digital display composite vacuum gauge (ZDF-5227A) equipped with vacuum carbon tube furnace is ±1 °C and ±1 pct, respectively. Finally, the cooled samples were weighed for the calculation of reduction ratio by Eq. [1] and prepared for chemical analysis of P content (Quinoline phosphomolybdate gravimetric method was used to determine the P content of reduced samples, and the detailed operation method refers to references.^[28,29]) for calculation of volatilization ratio of P by Eq. [2], XRD analysis, SEM appearance, and EDS.

$$\theta = \frac{m_1 - m_2 - m_3 + (M - M_0)}{m_1 - m_3} \times 100 \text{ pct} \quad [1]$$

Generally speaking, the weight loss ratio can characterize the degree of reduction without metal volatilization for the carbothermal reduction of solid-solid reaction. However, in this study, the reduced phosphorus volatilized in gaseous form, so the volatile phosphorus was taken into account when calculating the reduction ratio.

$$\eta = \frac{M - M_0}{M} \times 100 \text{ pct} \quad [2]$$

where θ is the reduction ratio of phosphate ore (pct), m_1 , m_2 , and m_3 are masses of samples before heating, samples after heating, and binder (g). η is volatilization ratio of P (pct), and M_0 and M are masses of P in

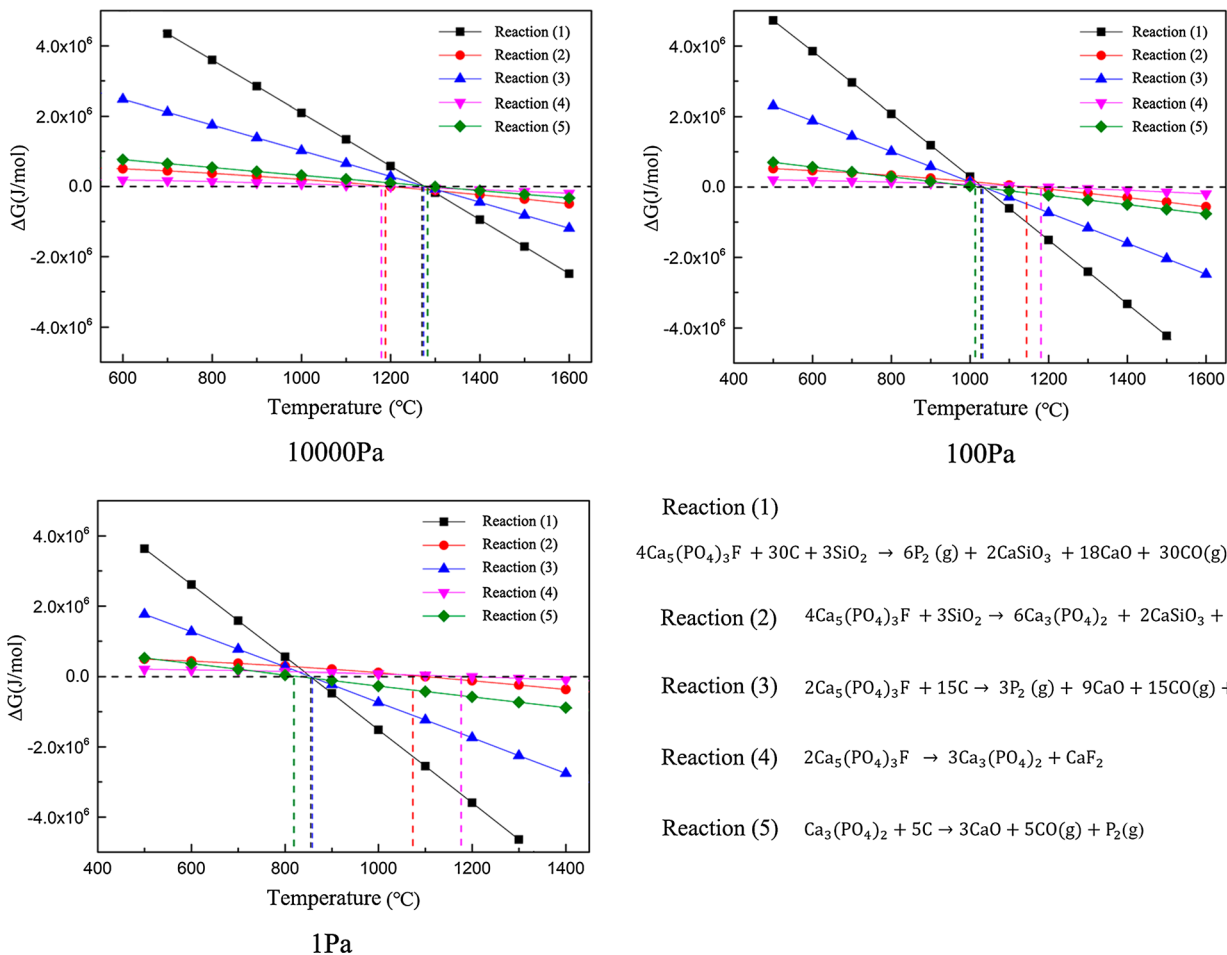


Fig. 1—Variations in Gibbs free energy as a function of pressure.

Table I. Chemical Composition of Raw Materials (Wt Pct)

| | | | | | | | | | | |
|---------------|-------|-------------------------------|-------|------------------|--------------------------------|--------------------------------|------------------|--------------------------------|-------------------|------------------|
| Phosphate Ore | CaO | P ₂ O ₅ | F | SiO ₂ | Fe ₂ O ₃ | MgO | K ₂ O | Al ₂ O ₃ | Na ₂ O | |
| | 49.08 | 28.89 | 1.42 | 5.04 | 2.15 | 1.72 | 0.32 | 0.96 | 0.11 | |
| Coke | S | P | FC | Volatile | Ash | Ash | | | | |
| | 0.65 | 0.12 | 83.66 | 2.22 | 14.12 | Fe ₂ O ₃ | CaO | Al ₂ O ₃ | MgO | SiO ₂ |
| | | | | | | 8.91 | 6.01 | 22.26 | 2.16 | 47.79 |

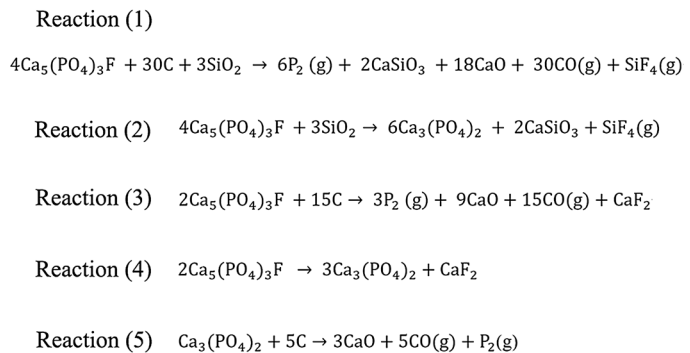
FC = 100 pct - M_{Ash} - M_{volatile} . “FC” represents the fixed carbon content in coke.

samples after reduction and P in samples before reduction (g). ($M - M_0$) is the mass of phosphorus which has evaporated.

III. RESULTS AND DISCUSSION

A. Effect of Temperature on Reduced Samples

Variations in reduction ratio, volatilization ratio of P, and pressure as a function of temperature are shown in Figure 5. The gas (mainly phosphorus vapor and CO) produced by the reduction reaction would cause the change of the pressure in the furnace. As can be seen from Figure 5, the reaction began to take place in large



quantities after 1250 °C. The reduction ratio of the sample and volatilization ratio of P increased with temperature at the range of 1100 °C to 1400 °C. And this tendency accelerated evidently above 1250 °C. The reduction ratio and volatilization ratio of P were 28.07 and 36.5 pct at 1400 °C.

B. SEM and EDS Analysis of Reduced Samples

The surface appearance and EDS analysis of reduced samples are shown in Figure 6. Four EDS analyses were carried out on the points of different regions with the same composition, and then the average atomic percentage of each element was obtained. In reduction samples at different temperatures, there was no obvious

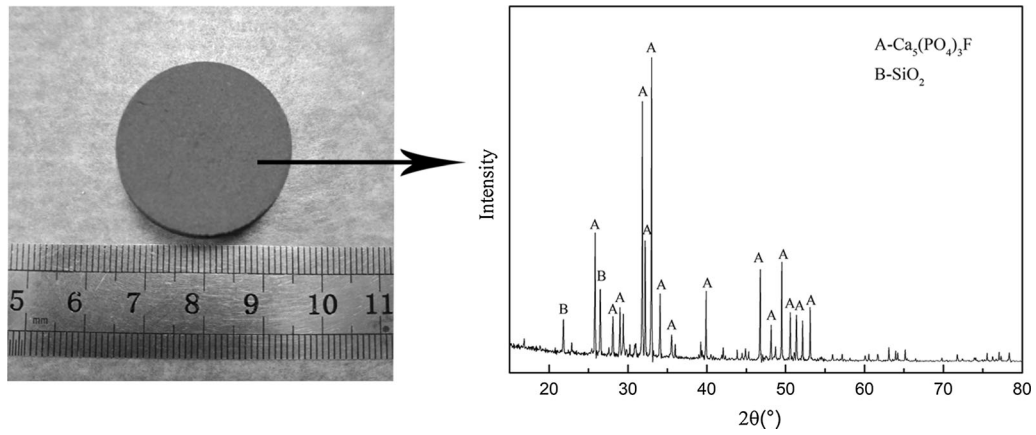


Fig. 2—XRD diagram of raw ore.

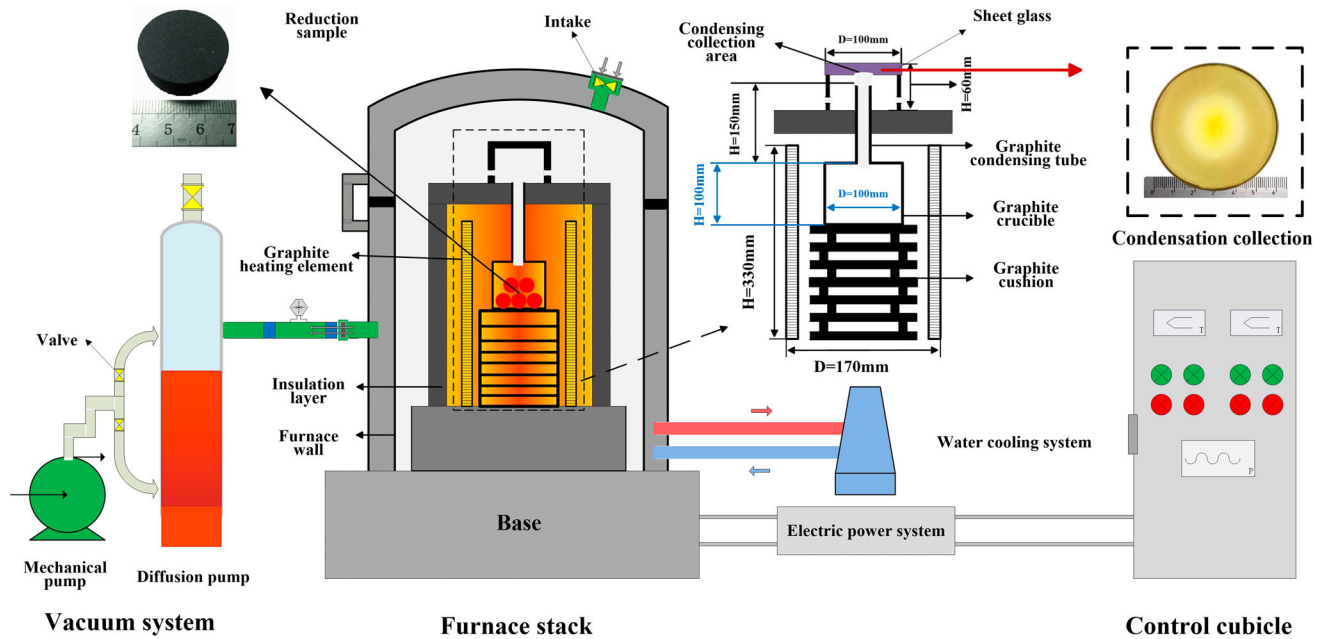


Fig. 3—Schematic diagram of vacuum carbon tube furnace.

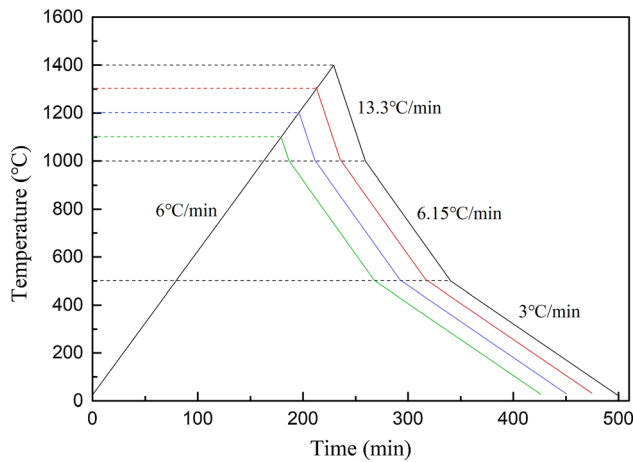


Fig. 4—Heating and cooling curves of samples.

change in the percentage of each atom in A, B, and C three areas. It can be seen that the areas of A were unreacted $\text{Ca}_5(\text{PO}_4)_3\text{F}$ and some calcium salts, the areas of B composition were ferrophosphorus and some ferroalloy, the areas of C were silicate and a small part of magnesium oxides, and the black areas were coke. A area and coke in the sample at 1200 °C showed obvious blocky structure. With the increase of temperature and the deepening of reduction, the particles of A area and coke in the reduced samples at 1300 °C and 1400 °C were obviously finer, and the coke was reticulated in the A area. This is due to the reduction at the two-phase interface and the formation of gas, which lead to the decomposition and refinement of the A area and coke particles. B and C areas, as the products, were mainly scattered at the particle contact interface of A area and coke.

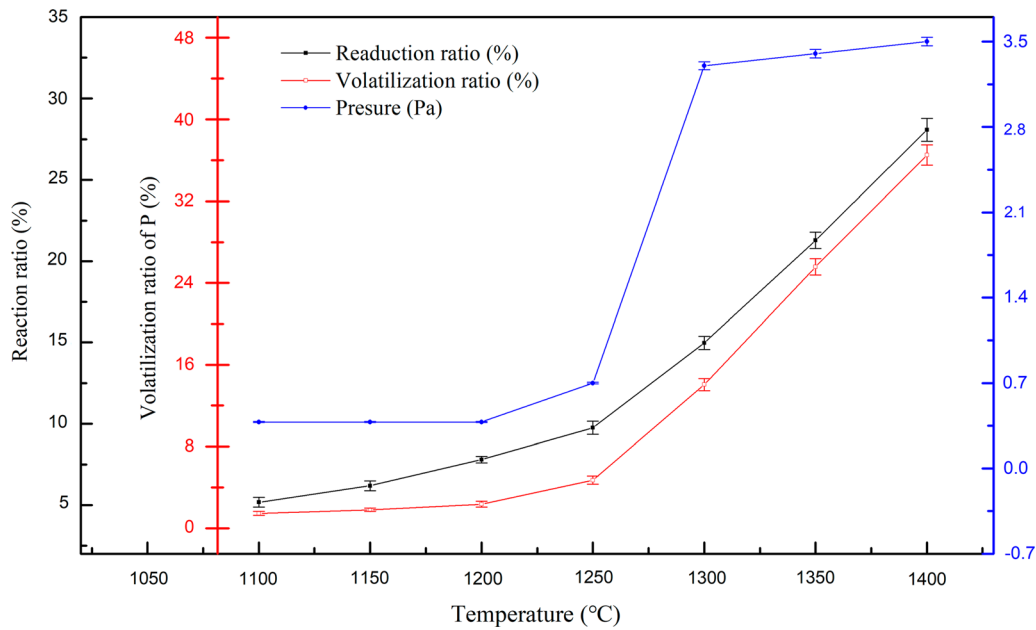


Fig. 5—Variations in reduction ratio, volatilization ratio of P, and pressure as a function of temperature.

C. X-ray Diffraction Analysis of Reduced Samples

XRD analysis results (based on the results of SEM and EDS analysis) are shown in Figure 7 and Table II. The diagram shows that the main phases in the raw ore were $\text{Ca}_5(\text{PO}_4)_3\text{F}$ and SiO_2 . The SiO_2 diffraction peak disappeared at 1100 °C to 1250 °C, the main phases of samples after reduction were $\text{Ca}_5(\text{PO}_4)_3\text{F}$, $\text{Ca}_3(\text{PO}_4)_2$, and CaSiO_3 , and the intensity of each diffraction peak showed no obvious change. At 1300 °C, the CaO diffraction peak appeared, and the main phases of samples after reduction were $\text{Ca}_5(\text{PO}_4)_3\text{F}$, $\text{Ca}_3(\text{PO}_4)_2$, CaO , and CaSiO_3 . There was no new phase forming above 1300 °C. The diffraction peak of $\text{Ca}_5(\text{PO}_4)_3\text{F}$ decreased gradually, whereas the diffraction peak of CaO increased gradually.

IV. KINETIC ANALYSIS

For the research of non-isotherm kinetics at a constant heating rate, the reaction rate of heterogeneous reaction can be obtained by Eq. [3]: [30–32]

$$\frac{d\alpha}{dt} = \beta \frac{d\alpha}{dT} = A \exp\left(\frac{-E}{RT}\right) f(\alpha) \quad [3]$$

where t , β , T , A , R , E , and $f(\alpha)$ are time, heating rate, temperature, pre-exponential factor, gas constant, activation energy, and differential mechanism function, respectively. The integral mechanism function ($G(\alpha)$) can be described as Eq. [4] through deformation:

$$G(\alpha) = \int_0^\alpha \frac{d\alpha}{f(\alpha)} = \frac{A}{\beta} \int_{T_0}^T \exp\left(\frac{-E}{RT}\right) dT \quad [4]$$

$$T = T_0 + \beta t \quad [5]$$

where T_0 is the initial temperature (room temperature).

Nowadays, several methods are used to verify each other to obtain dynamic parameters during the study of non-isothermic dynamics, which can determine more reliable mechanism function ($G(\alpha)$) and dynamic parameters. Han *et al.* [33,34] obtained the most reliable kinetic parameters by mutual verification of Flynn–Wall–Ozawa and Kissinger–Akahira–Sunose methods. Lv *et al.* [35,36] obtained the best kinetic parameters by mutual verification of Coats–Redfern [37] and Šatava–Šesták methods. [38] Based on this, the study will use this method to character the non-isothermal kinetics of carbothermal reduction of low-grade phosphate ore in vacuum.

Coats–Redfern integral method:

$$\ln\left(\frac{G(\alpha)}{T^2}\right) = \ln\left[\frac{AR}{\beta E} \left(1 - \frac{2RT}{E}\right)\right] - \frac{E}{RT} \quad [6]$$

Šatava–Šesták integral method:

$$\lg G(\alpha) = \lg\left(\frac{AE}{R\beta}\right) - 2.315 - 0.4567 \frac{E}{RT} \quad [7]$$

The integral mechanism function expressions used in the work are shown in Table III.

A. Data Correction

Because the samples were reduced in vacuum, it is impossible to take out the samples for quick cooling after reduction. Therefore, we set the cooling rate of the vacuum furnace to the maximum (the cooling rate was very fast at this time, and the heating and cooling curves of samples are shown in Figure 4). And the reduction ratio and phosphorus volatilization ratio were corrected in the non-isothermal kinetic study. The reduction and

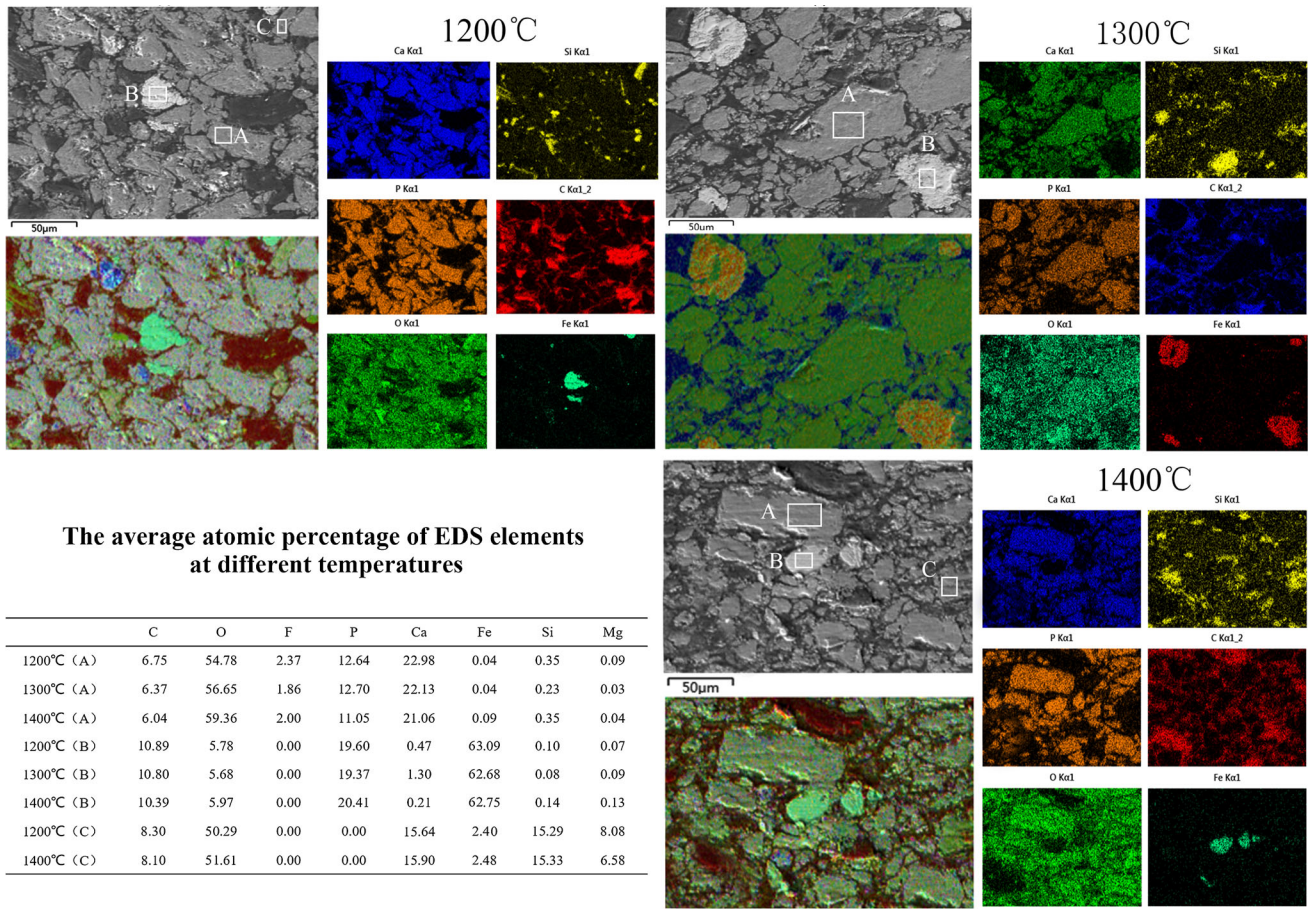


Fig. 6—The surface appearance and EDS analysis of the reduced samples.

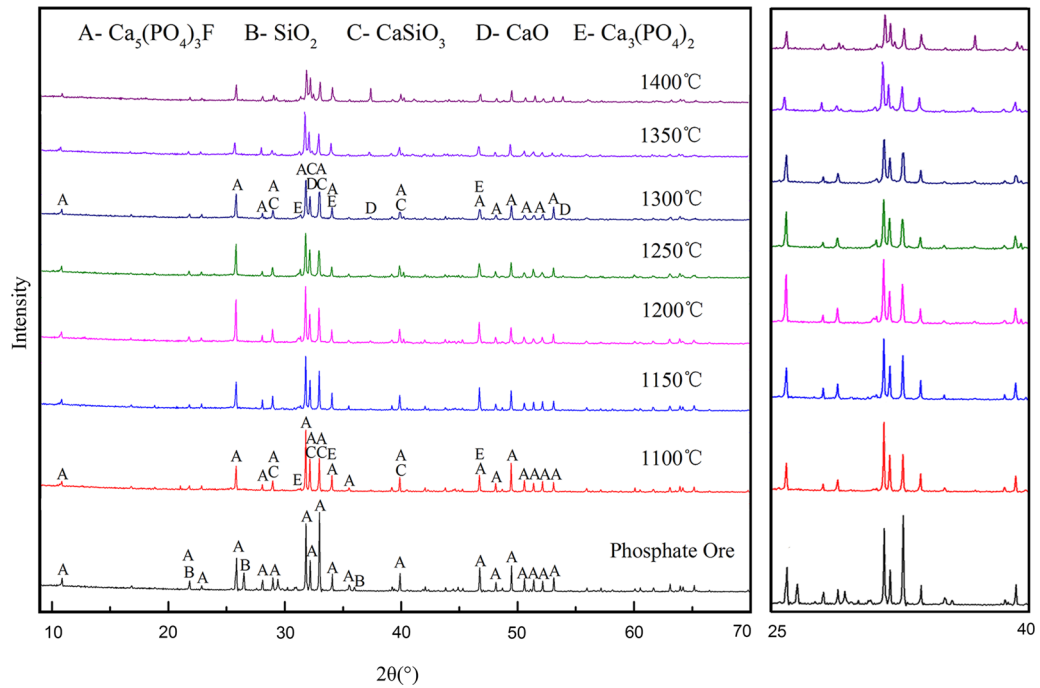


Fig. 7—XRD analysis of the reduced samples.

phosphorus volatilization in the cooling process were quantified by this method and subtracted from the original data. Finally, the corrected data were brought into the non-isothermal kinetic equations. The specific methods are as follows:

Let α be the change of phosphorus volatilization ratio, β the correction value of phosphorus volatilization ratio, γ the measured value of phosphorus volatilization ratio, and δ the unit temperature. Assuming that we have determined the phosphorus volatilization ratio and reduction ratio of $1400/\delta$ reduction samples, and the phosphorus volatilization ratio of per unit δ temperature stage was constant. Then each unit δ temperature stage contains a heating process volatilization α_{heating} and a cooling process volatilization α_{cooling} . t_{heating} and t_{cooling} are the time spent in heating and cooling processes of per unit δ temperature stage, respectively. Then,

$$\alpha_{(1400-\delta)\sim 1400^\circ\text{C cooling}} = \left(\gamma_{1400^\circ\text{C}} - \gamma_{(1400-\delta)^\circ\text{C}} \right) \times \frac{t_{\text{cooling}}}{t_{\text{heating}} + t_{\text{cooling}}} \quad [8]$$

$$\alpha_{(1400-2\delta)\sim(1400-\delta)^\circ\text{C cooling}} = \left(\gamma_{(1400-\delta)^\circ\text{C}} - \gamma_{(1400-2\delta)^\circ\text{C}} \right) \times \frac{t_{\text{cooling}}}{t_{\text{heating}} + t_{\text{cooling}}} \quad [9]$$

$$\alpha_{0\sim\delta^\circ\text{C cooling}} = (\gamma_{\delta^\circ\text{C}} - \gamma_{0^\circ\text{C}}) \times \frac{t_{\text{cooling}}}{t_{\text{heating}} + t_{\text{cooling}}} \quad [10]$$

And,

$$\begin{aligned} & \beta_{1400^\circ\text{C}} = \gamma_{1400^\circ\text{C}} \\ & - [\alpha_{(1400-\delta)\sim 1400^\circ\text{C cooling}} + \alpha_{(1400-2\delta)\sim(1400-\delta)^\circ\text{C cooling}} + \dots + \alpha_{1000\sim(1000+\delta)^\circ\text{C cooling}}] \\ & - [\alpha_{(1000-\delta)\sim 1000^\circ\text{C cooling}} + \alpha_{(1000-2\delta)\sim(1000-\delta)^\circ\text{C cooling}} + \dots + \alpha_{500\sim(500+\delta)^\circ\text{C cooling}}] \\ & - [\alpha_{(500-\delta)\sim 500^\circ\text{C cooling}} + \alpha_{(500-2\delta)\sim(500-\delta)^\circ\text{C cooling}} + \dots + \alpha_{0\sim\delta^\circ\text{C cooling}}] \\ & = \gamma_{1400^\circ\text{C}} - 31.09\text{pct} \times [\gamma_{1400^\circ\text{C}} - \gamma_{1000^\circ\text{C}}] - 49.38\text{pct} \times [\gamma_{1000^\circ\text{C}} - \gamma_{500^\circ\text{C}}] \\ & \quad - 66.67\text{pct} \times [\gamma_{500^\circ\text{C}} - \gamma_{0^\circ\text{C}}] \\ & = 24.94\text{pct} \end{aligned} \quad [11]$$

In the same way, all the correction values of phosphorus volatilization ratio and reduction ratio of samples were obtained, as shown in Table IV. Finally, the corrected data were brought into the kinetic formula to fit.

Table II. Main Phases of Reduced Samples at Different Temperature

| T (°C) | Main Phases |
|--------------------|--|
| Phosphate Ore | Ca ₅ (PO ₄) ₃ F, SiO ₂ |
| 1100 °C to 1250 °C | Ca ₅ (PO ₄) ₃ F, Ca ₃ (PO ₄) ₂ , CaSiO ₃ |
| 1300 °C to 1450 °C | Ca ₅ (PO ₄) ₃ F, Ca ₃ (PO ₄) ₂ , CaO, CaSiO ₃ |

B. Kinetic Analysis of Integral Reduction Samples

The reduction ratio was considered as the reduction degree of the sample. Linear fitting of integral expressions listed in Table III was carried out by Eqs. [6] and [7], respectively. As shown in Table V and Figure 8, an identical integral expression which has the highest fitting precision in fitting results was selected. And then, the kinetic parameters were obtained and listed in Table VI. Therefore, in the process of carbothermal reduction of low-grade phosphate ore in vacuum, the integral and differential mechanism function expressions of unitary reduction samples were $G(a) = 1 - (1 - a)^4$ and $f(a) = 1/4(1 - a)^{-3}$ by mutual verification of Coats–Redfern, and Šatava–Šesták methods, respectively. The reduction process was under the control of the Shrinking core model. The activation energy of unitary reduction was $74.54 \pm 10.39 \text{ kJ/mol}$ based on the two methods. The reduction process was mainly controlled by the phase boundary reaction. CaSiO₃, CaO, and other products attached between the reactant and coke were increasing with time, which limited the progress of the reaction.

C. Kinetic Analysis of Phosphorus Volatilization

The volatilization ratio of P in the reduction process was taken as the reduction degree of P. Linear fitting of integral expressions listed in Table III was carried out by Eqs. [6] and [7], respectively. As shown in Table VII

Table III. Common Integral Mechanism Function Expressions^[30,39,40]

| Reaction Model | Integral $G(a)$ |
|-----------------------------|--|
| 1-D Diffusion | α^2 |
| 2-D Diffusion (Valensi) | $\alpha + (1 - \alpha) \ln(1 - \alpha)$ |
| 3-D Diffusion (G-B) | $(1 - 2/3\alpha) - (1 - \alpha)^{2/3}$ |
| 3-D Diffusion (Jander) | $\left[\frac{1 - (1 - \alpha)^{1/3}}{1/3} \right]^{1/2} (n = 1/2, 2)$ |
| 2-D Diffusion (Jander) | $\left[\frac{1 - (1 - \alpha)^{1/2}}{1/2} \right]^2$ |
| 3-D Diffusion (anti-Jander) | $\left[\frac{(1 + \alpha)^{1/3} - 1}{1/3} \right]^2$ |
| Avrami-Erofeev | $-\ln(1 - \alpha)$ |
| Avrami-Erofeev | $[-\ln(1 - \alpha)]^n (n = 1/4, 1/3, 1/2, 2/3, 2, 3, 4)$ |
| Shrinking Core Model | $1 - (1 - \alpha)^n (n = 1/4, 1/3, 1/2, 2, 3, 4)$ |
| Mampel Power Law | $\alpha^n (n = 1/4, 1/3, 1/2, 1, 3/2)$ |
| Chemical Reaction | $(1 - \alpha)^{-1}$ |
| Chemical Reaction | $(1 - \alpha)^{-1} - 1$ |
| Chemical Reaction | $(1 - \alpha)^{-1/2}$ |

Table IV. The Reduction Ratio and Phosphorus Volatilization Ratio After Correction (Pct)

| Temperature(°C) | 0 | 500 | 1000 | 1100 | 1150 | 1200 | 1250 | 1300 | 1350 | 1400 |
|----------------------|---|------|------|------|------|------|------|-------|-------|-------|
| Before Correction | | | | | | | | | | |
| Reduction Ratio | 0 | 0.46 | 3.74 | 5.17 | 6.19 | 7.86 | 9.76 | 14.97 | 21.28 | 28.07 |
| Volatilization Ratio | 0 | 0.08 | 1.08 | 1.46 | 1.81 | 2.36 | 4.72 | 14.05 | 25.57 | 36.50 |
| After Correction | | | | | | | | | | |
| Reduction Ratio | — | — | — | 2.80 | 3.50 | 4.65 | 5.96 | 9.55 | 13.90 | 18.57 |
| Volatilization Ratio | — | — | — | 0.80 | 1.04 | 1.42 | 3.05 | 9.48 | 17.41 | 24.94 |

Table V. Integral and Differential Expressions of Mechanism Functions of the Unitary Reduction

| Reaction Model | G(a) (Integral Mechanism Function) | f(a) (Differential Mechanism Function) |
|----------------------|------------------------------------|--|
| Shrinking Core Model | $1 - (1 - \alpha)^4$ | $1/4(1 - \alpha)^{-3}$ |

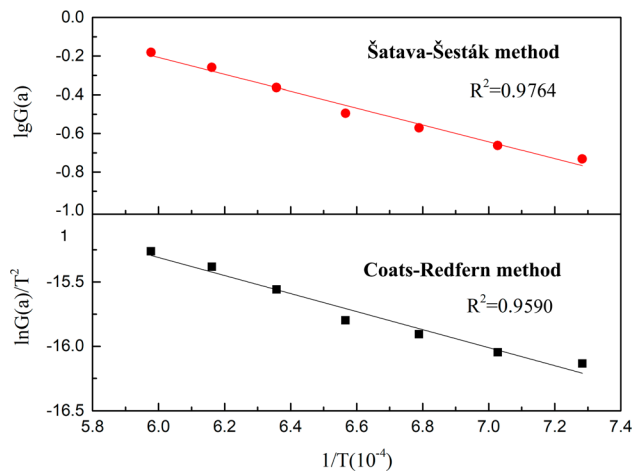


Fig. 8—Fitting diagram of the mechanism function of the unitary reduction.

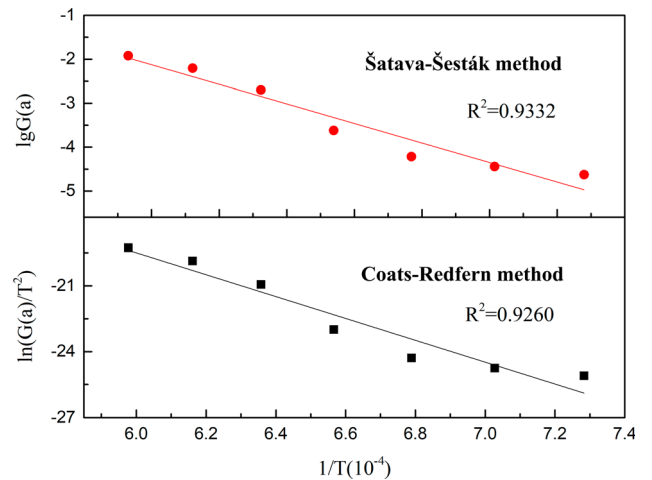


Fig. 9—Fitting diagram of the mechanism function of P volatilization.

Table VI. Kinetic Parameters of the Unitary Reduction

| | Coats-Redfern method | Šatava-Šesták method | Average | Standard Error |
|--------------------------------------|----------------------|----------------------|---------|----------------|
| Activation Energy E (kJ/mol) | 64.16 | 84.93 | 74.54 | 10.39 |
| Pre-exponential A (s ⁻¹) | 1.19 | 52.88 | 27.03 | 25.85 |

Table VII. Integral and Differential Expressions of Mechanism Functions of P Volatilization

| Reaction Model | G(a) (Integral Mechanism Function) | f(a) (Differential Mechanism Function) |
|-----------------------------|------------------------------------|--|
| 3-D diffusion (anti-Jander) | $[(1 + a)^{1/3} - 1]^2$ | $3/2(1 + a)^{2/3}[(1 + a)^{1/3} - 1]^{-1}$ |

Table VIII. Kinetic Parameters of the Volatilization Process

| | Coats-Redfern Method | Šatava-Šesták Method | Average | Standard Error |
|--------------------------------------|-----------------------|-----------------------|-----------------------|--------------------|
| Activation Energy E (kJ/mol) | 414.62 | 418.24 | 416.43 | 1.81 |
| Pre-exponential A (s ⁻¹) | 1.01×10^{10} | 1.41×10^{10} | 1.21×10^{10} | 2.00×10^9 |

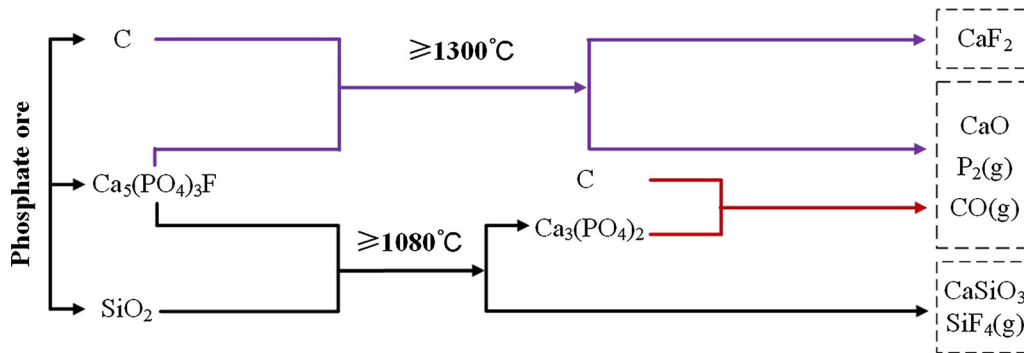


Fig. 10—Vacuum carbothermal reduction process of phosphate ore.

and Figure 9, an identical integral expression which has the highest fitting precision in fitting results was selected. And then, the kinetic parameters were obtained and listed in Table VIII. Therefore, in the process of P volatilization, the integral and differential mechanism function expressions were $G(a) = [(1 + a)^{1/3} - 1]^2$ and $f(a) = 3/2(1 + a)^{2/3}[(1 + a)^{1/3} - 1]^{-1}$ by mutual verification of Coats-Redfern and Šatava-Šesták methods, respectively. The volatilization process of P was under the control of the 3-D diffusion (anti-Jander). The activation energy of P volatilization was 416.43 ± 1.81 kJ/mol based on the two methods. Therefore, the restrictive section was the diffusion of coke to the surface of reactants and the escaping process of phosphorus vapor through the reaction layer.

V. MECHANISM ANALYSIS

A. Analysis of the Reduction Process

A study^[23] showed that Ca₅(PO₄)₃F is more likely to react with SiO₂ compared with C. The reduction process of carbothermal reduction of low-grade phosphate ore in vacuum was obtained via the analyses above. Figure 10 shows that Ca₅(PO₄)₃F first reacted with a small amount of SiO₂ in the ore sample at 1080 °C to form Ca₃(PO₄)₂, CaSiO₃, and SiF₄ (escaped in the form of gas). Then, Ca₃(PO₄)₂ was reduced by C. When the temperature reached approximately 1300 °C, a large number of Ca₅(PO₄)₃F in the ore sample began to react with C to form CaO, P₂(g), CO(g), and CaF₂.

The main reactions were as follows:

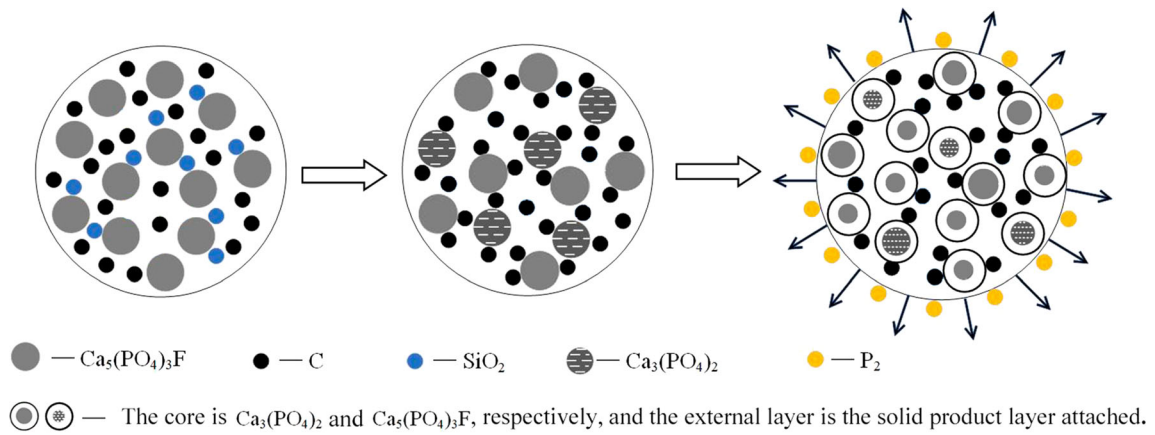
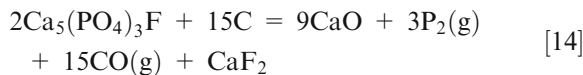
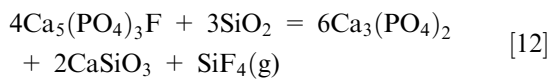


Fig. 11—Reduction mechanism diagram of phosphate ore.



The reaction of $\text{Ca}_5(\text{PO}_4)_3\text{F}$ and SiO_2 was calculated by using FactSage7.2 software's Reaction module. A conclusion that the initial reaction temperature is 1080 °C at the pressure of 1Pa, $\Delta G = -7.3235 \times 10^3 \text{J/mol}$ was drawn.

B. Analysis of the Reduction Mechanism

The reduction mechanism of phosphate ore during vacuum carbothermal reduction was shown in Figure 11. When the reaction conditions were reached, $\text{Ca}_5(\text{PO}_4)_3\text{F}$ first defluorinated with SiO_2 to form $\text{Ca}_3(\text{PO}_4)_2$, and then the reduction began at the two-phase interface of $\text{Ca}_3(\text{PO}_4)_2$ and C. As SiO_2 was depleted, $\text{Ca}_5(\text{PO}_4)_3\text{F}$ in the phosphorite directly reacted with C (the initial reaction temperature was about 1300 °C under 1Pa). The reduction was a typical gas-solid phase reaction, which was gradually advanced inward. Solid-state products such as CaSiO_3 and CaO were increasing and attached to the reactant surface with reaction. And a shrinking core consisting of unreacted reactants existed in the reduced ore until the end of the reaction. The presence of this solid-state product layer reduced the contact area between $\text{Ca}_5(\text{PO}_4)_3\text{F}$, $\text{Ca}_3(\text{PO}_4)_2$, and carbon, limiting the reaction to proceed. Gaseous yellow phosphorus continuously diffused from the surface of reactants to the surface of the sample and escaped with CO. The diffusion of yellow phosphorus was the restrictive section of its volatilization process.

VI. CONCLUSION

The non-isothermal kinetics and reduction process of carbothermal reduction of low-grade phosphate ore were investigated in vacuum by XRD, SEM, EDS, chemical analysis, and FactSage 7.2. The conclusions were summarized as follows:

- (1) The reduction ratio of the samples and volatilization ratio of P increased with temperature at the range of 1110 °C to 1400 °C. The tendency accelerated evidently above 1250 °C and the reaction began in large quantities. The reduction ratio and volatilization ratio of P were 28.07 and 36.5 pct at 1400 °C.
- (2) Through the mutual verification of Coats-Redfern and Šatava-Šesták methods, it is concluded that the unitary reduction process was under the control of the shrinking core model, and the activation energy of unitary reduction was $74.54 \pm 10.3 \text{ kJ/mol}$. The volatilization of P was under the control of the 3-D diffusion (anti-Jander), and the activation energy was $416.43 \pm 1.81 \text{ kJ/mol}$.
- (3) $\text{Ca}_5(\text{PO}_4)_3\text{F}$ first reacted with a small amount of SiO_2 in the ore sample at 1080 °C to form $\text{Ca}_3(\text{PO}_4)_2$, CaSiO_3 , and SiF_4 (escaped in the form of gas). Then, $\text{Ca}_3(\text{PO}_4)_2$ was reduced by C. When the temperature reached approximately 1300 °C, a large number of $\text{Ca}_5(\text{PO}_4)_3\text{F}$ in ore sample began to react with C to form CaO , $\text{P}_2(\text{g})$, $\text{CO}(\text{g})$, and CaF_2 .

ACKNOWLEDGMENTS

The authors acknowledge the support of the National Natural Science Foundation of China (Grant Nos. 51664003, 52064010, U1812402, and 51664004), High-level Talents Studying Abroad Program for Innovation and Entrepreneurship No. (2019)08, and Guizhou Province-Guizhou Institute of Technology Natural Science Foundation of China (LH Word No. [2016]7098)

REFERENCES

1. X. Zhao, M.D. Cai, Q.Q. Dong, Y.J. Li, and J.B. Shen: *J. Plant Nutr. Fertilizers*, 2018, vol. 24 (04), pp. 1121–30.
2. J. Jiang: *Multipurp. Util. Miner. Resour.*, 2014, vol. 04, pp. 16–19.
3. J.Y. Li, X. Tong, B. Han, H.Z. Lv, and D.D. Xie: *Util. Miner. Resour.*, 2015, vol. 05, pp. 57–62.
4. J.G. Zhu and Y.L. Dai: *Guizhou Chem. Ind.*, 2011, vol. 36 (03), pp. 21–26.
5. M.A. Abdel-Zaher: *Int. J. Miner. Process.*, 2008, vol. 85 (04), pp. 59–84.
6. L.N. Ni, H.P. Li, K.B. Luo, and Y. Su: *Sci. Technol. Chem. Ind.*, 2013, vol. 21 (01), pp. 58–62.
7. M. Gharabaghi, M. Irannajad, and M. Noaparast: *Hydrometallurgy*, 2010, vol. 103 (1–4), pp. 96–107.
8. R.Y. Wang, X.P. Yu, Z.C. Guo, X.M. Yang, and D.G. Wang: *Chin. J. Process Eng.*, 1997, vol. 04, pp. 76–79.
9. Z.C. Guo, D.G. Wang, and Z.H. Xu: *Chin. J. Process Eng.*, 1994, vol. 03, pp. 189–95.
10. Q. Li, B. Hu, Y.X. Wu, F. J, Q.F. Tian, Y. Li and S.F. He: *J. Chem. Eng. Chin. Univ.*, 2014, vol. 28(04), pp. 905–10.
11. C. Ma, B. Hu, Y.X. Wu, and F. Jin: *Ind. Miner. Process.*, 2014, vol. 43 (03), pp. 5–8.
12. F. Jin, Y.Z. Yang, C. Ma, X.L. Zhu, J.R. Wang, and Y.X. Wu: *Inorg. Chem. Ind.*, 2013, vol. 45 (11), pp. 29–32.
13. Q. Li, B. Hu, Y.X. Wu, Q.F. Tian, F. Jin, Y. Li, and C. Ma: *Chem. Eng.*, 2013, vol. 41 (04), pp. 51–56.
14. B. Hu, Q. Li, Y. Hu, F. Jin, and Y.X. Wu: *Ind. Miner. Process.*, 2012, vol. 41 (12), pp. 1–3 + 46.
15. J.W. Tang, F.J. Lan, Q.X. Hua, Y. Liu, L. Liu, and B.M. Wang: *Ind. Miner. Process.*, 2016, vol. 45 (09), pp. 9–12 + 19.
16. V. Garcia-Osorio and B.E. Ydstie: *Chem. Eng. Sci.*, 2004, vol. 59 (10), pp. 2053–64.
17. M.S. Walker and R.J. Fruehan: *Metall. Trans. B*, 2013, vol. 44 (4), pp. 853–61.
18. M.S. Walker and R.J. Fruehan: *Metall. Trans. B*, 2014, vol. 45 (4), pp. 1565–72.
19. C. Wieckert, R. Palumbo, and U. Frommherz: *Energy*, 2004, vol. 29 (5/6), pp. 771–87.
20. W.P. Yan, L.C. Li, R. Huang, P.S. Liu, K.S. Luo, S.L. Li, and S.S. Long: *Guangzhou Chem. Ind.*, 2017, vol. 45 (12), pp. 101–103 + 164.
21. X. Qian, R. Huang, P.S. Liu, X.D. Lv, and J.Z. Zhang: *Chin. J. Vac. Sci. Technol.*, 2017, vol. 37 (7), pp. 739–43.
22. Q.H. Wu, R. Huang, X.D. Lv, X. Qian, L. Liu and J.Z. Zhang: *Mater. Res. Express*, 2019, vol. 6.
23. R.F. Cao, Y. Li, J.P. Xia, W.L. Li, and W.Y. Han: *J. Chem. Eng. Chin. Univ.*, 2019, vol. 33 (02), pp. 372–79.
24. G.Y. Zheng, R.F. Cao, Y. Li, J.P. Xia and Z.J. Chen: *Silicon*, 2019.
25. Q.X. Li, J. Lv, and B. Jin: *Vacuum*, 2014, vol. 51 (06), pp. 56–58.
26. Y.C. Liu, Q.X. Li, and Z.Z. Qiu: *Chin. J. Vac. Sci. Technol.*, 2013, vol. 33 (03), pp. 293–96.
27. Y.C. Liu, Q.X. Li, and Y.C. Liu: *Vacuum*, 2012, vol. 49 (03), pp. 84–87.
28. K.J. Chen, L.Y. Feng, J.J. Hu, Q. Tian, S.J. Yang, and M. Chen: *South China Agric.*, 2020, vol. 24 (14), pp. 160–62.
29. China National Standards (Phosphate rock and concentrate–Determination of silicon dioxide content–Gravimetric and volumetric methods, Beijing, 1995). <http://openstd.samr.gov.cn/bzgk/gb/newGbInfo?hcno=2CD8171E5EBD83B7D2AD86855B451080>, Accessed 21 Dec 1995.
30. M.X. Huang, C.R. Zhou, and X.W. Han: *J. Therm. Anal. Calorim.*, 2013, vol. 113 (2), pp. 589–93.
31. M. Otero, L.F. Calvo, M.V. Gil, A.I. Garcia, and A. Morán: *Bioresour. Technol.*, 2008, vol. 99 (14), pp. 6311–19.
32. Y.S. Sun, Y.X. Han, X.C. Wei, and P. Gao: *J. Therm. Anal. Calorim.*, 2016, vol. 123 (1), pp. 703–15.
33. X.L. Han, F.L. Ding, Y.S. Qin, D.Y. Wu, H. Xing, Y. Shi, K.K. Song, and C.D. Cao: *Vacuum*, 2018, vol. 151, pp. 30–38.
34. T. Xu, Z. Jian, F. Chang, L. Zhuo, and T. Zhang: *Vacuum*, 2018, vol. 152, pp. 8–14.
35. X.D. Lv, R. Huang, Q.Z. Wu, B.J. Xu, and J.Z. Zhang: *Vacuum*, 2019, vol. 160, pp. 139–45.
36. R. Huang, X.D. Lv, Q.H. Wu, Q.Z. Wu, and Q.Z. Zhang: *Metall. Trans. B*, 2019, vol. 50B, pp. 816–24.
37. F. Šatava and J. Šesták: *J. Therm. Anal.*, 1975, vol. 8 (3), pp. 477–89.
38. A.W. Coats and J.P. Redfern: *J. Polym. Sci.*, 1965, vol. 3, pp. 917–20.
39. P. Li, Q.B. Yu, H.Q. Xie, Q. Qin, and K. Wang: *Energy Fuel.*, 2013, vol. 27 (8), pp. 4810–17.
40. P. Li, Q.B. Yu, Q. Qin, and W. Lei: *Ind. Eng. Chem. Res.*, 2012, vol. 51 (49), pp. 15872–83.

Publisher's Note Springer Nature remains neutral with regard to jurisdictional claims in published maps and institutional affiliations.